Tribology Transactions

ISSN: (Print) (Online) Journal homepage: www.tandfonline.com/journals/utrb20

Effect of Lubricant Properties and Contact Conditions on False Brinelling Damage

Rachel Januszewski, Victor Brizmer & Amir Kadiric

To cite this article: Rachel Januszewski, Victor Brizmer & Amir Kadiric (2023) Effect of Lubricant Properties and Contact Conditions on False Brinelling Damage, Tribology Transactions, 66:2, 350-363, DOI: 10.1080/10402004.2023.2183915

To link to this article: https://doi.org/10.1080/10402004.2023.2183915

TRIBOLOGY TRANSACTIONS
2023, VOL. 66, NO. 2, 350–363
https://doi.org/10.1080/10402004.2023.2183915

Effect of Lubricant Properties and Contact Conditions on False Brinelling Damage

Rachel Januszewski[a], Victor Brizmer[b], and Amir Kadiric[a]

[a]Department of Mechanical Engineering, Imperial College London, London, United Kingdom; [b]SKF Research and Technology Development, Houten, The Netherlands

ABSTRACT

False brinelling is a type of fretting wear that occurs in rolling bearings when the contacts of bearing rings and rolling elements are subjected to small-amplitude oscillatory motion. It manifests itself as deep craters with relatively polished bottoms that are evenly spaced around the bearing rings. This work investigates the influence of lubricant properties and contact conditions, including oil viscosity, applied load, and amplitude and frequency of oscillations, on the onset and progression of false brinelling damage. Experiments were conducted with AISI 52100 bearing steel specimens in a ball-on-flat configuration under small-amplitude oscillating conditions. A set of base oils and a group of custom-made greases with systematically varying properties were employed. Importantly, the same ball-on-flat setup was adapted to allow optical access to the contact by employing a sapphire disc instead of a steel one. This allowed direct observation of the damage onset and progression to better elucidate the mechanisms taking place. Additional experiments were conducted with the same lubricants on a thrust ball bearing rig and the observed trends were compared to those from the ball-on-disc setup. Results show that false brinelling damage initiates locally at discrete asperity microcontacts and then spreads relatively quickly with continued rubbing to cover the whole contact area. Oscillation amplitudes shorter than the Hertz contact width (A/D $<$ 1) were shown to be most damaging, while the damage reduces drastically for amplitudes larger than the Hertz contact width (A/D $>$ 1). For the more important case of A/D $<$ 1, oils and greases with lower viscosities produced less damage. Oils in general produced somewhat less damage than the equivalent lithium- or urea-thickened greases with the same base oil. Lower oscillation frequencies and lower contact pressures also produced less damage. The corresponding friction and electrical contact resistance measurements indicate that under these conditions of A/D $<$ 1 the contact operates under boundary lubrication at best but can intermittently approach effectively dry conditions, depending on lubricant properties and applied conditions. These observations indicate that the key variable that controls damage when the oscillation amplitude is less than the contact width is the ability of the lubricant to penetrate and remain in the oscillating contact. Therefore, lubricant properties and contact conditions that promote this penetration, which may be different from those that promote hydrodynamic film formation, can mitigate against false brinelling.

ARTICLE HISTORY
Received 31 July 2021
Accepted 19 February 2023

KEYWORDS
Fretting; false brinelling; wear; grease; bearing; oscillation

Introduction

False brinelling is a type of fretting wear that occurs in rolling bearings subjected to small-amplitude oscillations and manifests itself as distinct, evenly spaced craters on bearing raceways. A typical example of advanced false brinelling is shown in Fig. 1. It is caused by small-amplitude oscillations in the nonconformal contacts between the rolling elements and bearing raceways when bearings are nominally stationary. The oscillations within the contact are usually caused by some external source of vibration, for example, during transport of machines or in standby equipment located next to an operating machine. The craters replicate the shape of the ring-element contact and are spaced at the element pitch. The precise mechanisms of false brinelling are not entirely understood, but ultimately the damage is caused by significant metal-to-metal contact between the rolling element and the ring, which occurs due to the inability of the bearing lubricant to effectively penetrate the oscillating contact, and subsequent adhesive and other wear mechanisms taking place. In common with other types of fretting damage, false brinelling is associated with the formation of hard iron oxide debris that may remain trapped within the oscillating contact, thus facilitating further rapid wear through third-

CONTACT Rachel Januszewski rachel.januszewski12@imperial.ac.uk
Review led by N. Londhe.
Supplemental data for this article is available online at https://doi.org/10.1080/10402004.2023.2183915.

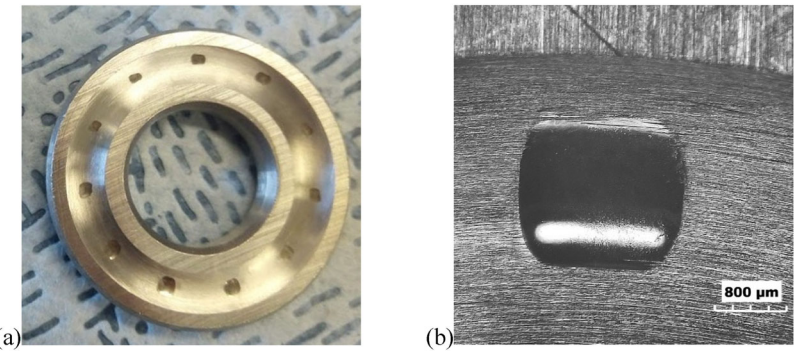

Figure 1. (a) False brinelling on a thrust ball bearing test specimen. (b) A magnified image of one of the craters from (a).

body wear mechanisms. False brinelling can lead to uneven running of the bearing, increased starting friction and bearing noise *(1)*, and can ultimately cause a premature bearing failure *(2)*.

False brinelling was reported in the literature as early as 1937. Almen *(3)* first investigated surface marks found on bearings in cars during transport by train. He recognized that these were similar in appearance to the craters found in true brinelling in the Brinell hardness test but that they were caused by different mechanisms, hence the term false brinelling. False brinelling is a tribological wear process, whereas true brinelling is caused by plastic deformation of a surface during an indentation process. It is this wear process that results in one clear distinction between false and true brinelling: the indentations caused by true brinelling show the original surface machining marks despite the macro plastic deformation of the surface *(4)*, whereas these have been rubbed off in the case of false brinelling resulting in a relatively polished, shiny surface. False brinelling continues to be an issue during transport of machinery as globalization sees equipment transported around the world, with risk of damage increasing with transport distances *(3)*. It is a recognized issue in standby machine units that are stored close to running equipment and hence subjected to vibration for prolonged periods of time. The damage is often discovered only when the standby equipment is put to use and the bearings are found to be noisy. More recently, false brinelling has been recognized as a major failure mode in two modern engineering applications, namely, wind turbine pitch bearings *(5)*, particularly in the designs where individual pitch control for each blade is employed *(6)*, and in hybrid vehicle bearings *(7, 8)*. Wind turbine pitch bearings can spend long periods of time under a nominally stationary condition while subjected to vibrations from the operating turbine, and when in actual operation, they oscillate through small angles, in the range of 5°, both of which increase the risk of false brinelling. In hybrid vehicles, one of the two power sources, either the internal combustion engine or the electric motor, is often stationary while being subjected to vibrations caused by the operating power train and/or from the moving vehicle.

False brinelling was recognized as a type of the more general damage mode of fretting wear in the 1960s *(1)*. The same wear mechanisms associated with small amplitude oscillations are responsible for both, but the term "false brinelling" is generally used to describe the manifestation of this type of damage in rolling element bearings. A differentiating feature of false brinelling is that it occurs under nominally lubricated conditions whereas many other examples of fretting occur under dry conditions, such as in blade roots of aero engines, in spline couplings and flange joints, or indeed in bearing ring–shaft interfaces. Under normal operating conditions, the lubricant in bearings, oil or grease, would form an elastohydrodynamic film that separates the surfaces and hence reduces the amount of metal-to-metal contact. However, under small-amplitude oscillations, lubricant entrainment to the contact is impaired and surface speeds are often low, so hydrodynamic film cannot be formed. Furthermore, in cases where the oscillating amplitude is smaller than the contact width in the sliding direction, parts of the contact are never exposed to the surroundings so that lubricant penetration is very difficult and even boundary lubrication may be diminished. Under these conditions, metal-to metal contact prevails, which leads to surface wear. This then leads to the formation of iron oxide debris that may not be expelled from the oscillating contact, thus facilitating enhanced wear rates via a third-body wear mechanism.

Campbell *(9)* and Pittroff *(1)* note an increased fretting resistance in bearing applications in the presence of lubricant. Shima et al. *(10)* suggest that a lubricant can have multiple effects under fretting conditions, including reduction of friction, reduction of oxygen access to the contact, which can restrict oxidation of both the worn contact surfaces and the metallic debris, and redistribution or removal of wear debris from the interface. Zhou *(11)* found that the coefficient of friction and the wear were lower under lubricated than under unlubricated fretting conditions and that wear occurs mainly during the initial stages of fretting. They further recognized that the ratio of the oscillation amplitude to Hertzian contact size in the sliding direction (A/D ratio) is an important factor governing lubricant access to the inner regions of a fretting contact and hence the propensity for fretting damage. Maruyama and Saitoh *(12)* showed that when the A/D ratio is larger than about 1.5, increasing oil viscosity can reduce fretting damage in bearings, while in the case of greases at these high oscillating amplitudes there appears to exist an optimum base oil viscosity that promotes hydrodynamic film formation while preventing starvation. It is therefore crucial to distinguish between the effects of

lubricant when A/D is less than 1, the "true" fretting conditions, and those when A/D is larger than 1. For A/D <1, it is the lubricant's ability to penetrate the oscillating contact and provide some level of boundary lubrication that influences the damage, whereas for A/D > 1, some hydrodynamic film may be formed, and in this case lubricant properties that promote formation of hydrodynamic film may help to reduce damage.

Although the existing literature on fretting and false brinelling recognizes the importance of the lubricant on the extent of damage as evident above, systematic studies into how specific lubricant properties affect fretting are very limited. This is particularly true for conditions where the A/D ratio is less than 1 and in the case of bearing greases; given that more than 90% of bearings are grease lubricated, this hinders the design of mitigating measures against false brinelling.

Besides the effects of lubricant, the influence of relevant contact conditions, such as contact pressure and stroke length, on general fretting damage have been investigated by several authors *(13–17)*. However, other than a few notable exceptions, including Grebe *(2)* and Schwack *(6)*, these studies do not consider many of the factors relevant to false brinelling in rolling bearings, including specific bearing steels, relatively high contact pressures, and the use of bearing greases. Additionally, there appears to be a lack of systematic investigations that isolate the influence of a single relevant variable at a time. This is at least in part likely to be due to multiple and interacting influencing factors. Indeed, Dobromirski *(18)* notes the difficulty in obtaining results for the influence of a single variable because of the synergy between different factors. Finally, much of what is known about the relevant mechanisms is indirectly inferred from the post-test inspection of damage and there is very little direct, in-situ observation of the sequence of events that leads to damage initiation and progression.

In view of this, the present work aims to (i) provide direct in-contact observations of the initiation and progression of false brinelling damage to better establish the sequence of events leading to damage and hence understand the mechanisms at play; (ii) provide new data and insights into the effects of relevant contact variables (stroke, frequency and contact pressure) on false brinelling using a systematic experimental approach able to isolate the influence of a single variable at a time; and (iii) systematically evaluate the effect of grease properties (base oil viscosity and grease thickener type) on false brinelling.

The results should serve to further our understanding of the relevant phenomena but are also of value in practice, either to help devise new predictive tools or to provide mitigating measures to existing false brinelling problems.

Experimental methods and materials

The present study makes use of two experimental setups: a modified high-frequency reciprocating rig (PCS HFRR) and a thrust ball bearing rig designed to perform bearing fretting tests according to the ASTM D4170 *(19)*, which evaluates "fretting wear protection by lubricating greases," commonly known as the Fafnir Fretting Wear Tester.

High-frequency reciprocating rig (HFRR)

Experiments to investigate the influence of various lubricant properties and contact conditions on the damage due to small amplitude oscillating motion were performed using a PCS Instruments high-frequency reciprocating rig (HFRR) shown in Fig. 2. In this rig a 6-mm-diameter ball specimen is reciprocated against the flat surface of a disc under oscillating amplitudes as low as 20 μm. Oscillating motion is provided by an electromagnetic vibrator. The drive system permits variation in both amplitude and frequency of oscillation and the normal load is varied mechanically using weights. A linear variable differential transducer measures linear displacement in order to control the stroke length, and a fretting flexure lock ensures accuracy at stroke lengths below 100 μm. The temperature of the test cell is controlled through a heater block. The system records frictional force and electrical contact resistance. The electrical contact resistance provides an indication of the prevalent lubrication conditions in the contact throughout the tests *(20)*, which greatly aids the interpretation of observed fretting wear trends.

HFRR experiments were conducted over a wide range of conditions listed in Table 1. Tests were designed to isolate

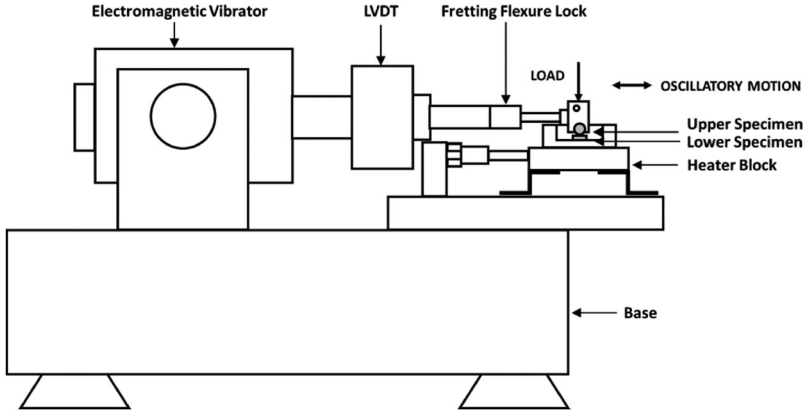

Figure 2. PCS Instruments HFRR rig employed here for false brinelling studies.

Table 1. Range of test conditions employed on the high-frequency reciprocating rig.

Variable	Tested values
Stroke length (μm)	**20**, 40, 60, 80, 100, 120, 140, 160
Maximum Hertz pressure (GPa)	0.65, 0.82, **1.04**, 1.30
Frequency (Hz)	50, **100**, 150
Sliding distance (m)	**14.4**
Test duration (hours)	Varied depending on stroke and frequency to obtain the specified total sliding distance of 14.4 m (e.g., at 20 μm stroke length and 100 Hz the test duration is 1 hour)
Test temperature (°C)	**25**

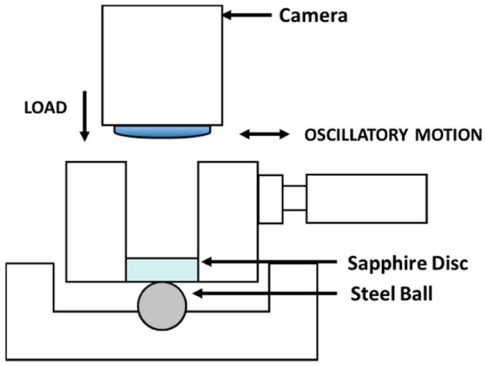

Figure 3. A schematic of the custom-made optical setup for the HFRR.

the influence of stroke length, frequency of oscillation, applied load and lubricant properties. Only one parameter was varied at a time within the specified range of values; when doing so, other variables were kept at the values shown in boldface in Table 1. To ensure like-for-like comparison of wear depth across tests at different strokes and frequencies, the test duration was varied as necessary to achieve the same total sliding distance of 14.4 m regardless of stroke length or frequency employed. For example, at 20 μm stroke length and 100 Hz the test duration is 1 hour, while at 20 μm and 50 Hz it is 2 hours.

The standard HFRR rig only records friction force averaged over 1 second, during which mulitple complete oscillations occur. Here, it was desired to observe the variation of friction force against displacement during a single oscillating cycle, a so-called "fretting loop." To achieve this, a slight modification was made to the setup to be able to record instantaneous friction force and displacement at high sampling rates by connecting one oscilloscope channel directly to the raw force output of the mechanical unit and a second oscilloscope channel to the raw displacement output.

To provide for direct observation of damage onset and progression, an additional custom-made setup was used where a sapphire flat was employed instead of the steel disc to enable optical access to the contact. This arrangement is shown schematically in Fig. 3. The setup is similar to that employed by Baker *(21)* in his studies into the transition between fretting and reciprocating sliding wear, and consists of a transparent sapphire disc oscillated against a AISI 52100 steel ball located below it with a camera located above the transparent disc to view the contact.

HFRR test procedure

Before each HFRR test, ball and disc specimens, specimen holders, and all attachments were cleaned thoroughly using isopropyl alcohol (IPA) and dried with air. They were then cleaned again using toluene and finally placed in a jar of IPA in an ultrasonic bath for 15 minutes. After removal from the bath, the specimens, holders and attachments were left to dry in air for at least 10 minutes.

The specimens were then fastened in their relevant holders and these holders were attached to the rig. The lubricant was then added to the test cell. For tests with oil, 2.0 ml of oil was put into the oil bath such that the ball and disc specimens were immersed in oil, and for tests with greases, 0.030 ± 0.005 g of grease was evenly spread over the whole surface of the disc specimen.

During the test, friction and contact resistance were recorded continuously, with the latter providing an indication of the lubrication conditions in the oscillating contact. Following the end of the test, specimens were removed for wear scar inspection. This was done by first using optical microscopy to provide general observations of the wear, followed by white light interferometry to quantify the size of the wear crater on the disc. The parameter chosen to characterize the extent of fretting wear is the maximum depth of the crater on the disc specimen. This maximum depth commonly occurs near the middle of the contact for all fretting tests, with the only exception being the cases with the largest stroke lengths employed here. This exception is related to the differences in wear mechanisms between fretting and gross sliding type contact conditions, which are discussed at length later. The disc wear scar depth was used here because wear occurs preferentially on the disc, owing to the fact that the ball hardness was higher than that of the disc, at 850 Hv and 755 Hv respectively (see Table 3). The maximum depth was obtained from three-dimensional (3D) profilometry measurements of the wear scars after suitable filtering. This ensures that any local, sharp features in the profiles are excluded and that any variations in the exact location of the maximum wear depth (which may be missed when using two-dimensional profilometry) are accounted for. Repeatability of the HFRR wear tests was found to be very good. Nevertheless, all reported HFRR wear results in this article are averages from at least three repeat tests under each set of conditions and all relevant plots also show the error bars derived from these repeats.

It should be noted that other parameters to describe generated wear were also explored in this study but were found to be less reliable than maximum wear depth. This included mass loss and wear scar volume. The mass loss was found to be inadequate to pick up the differences between different tests, probably due to the fact that the material mass lost in the present tests is relatively small. This measure may, however, be sufficient in other tests such as the standard Fafnir bearing tests (a selection of which was also conducted as part of this study and described later). The wear volume was obtained from the 3D profilometry measurements of the wear scars by fitting a reference plane below which the lost volume can be calculated by the profilometry software or

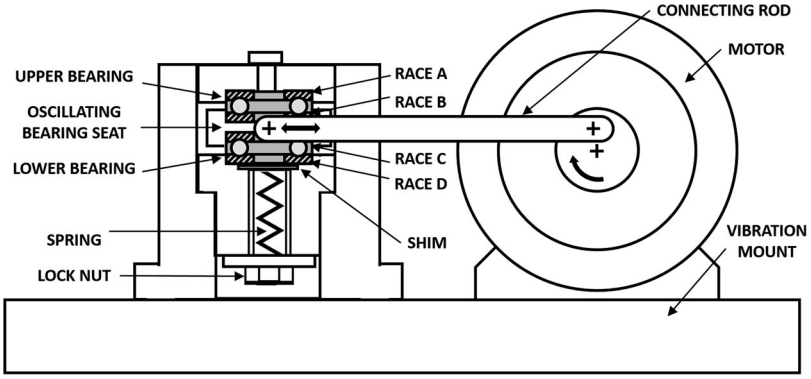

Figure 4. Thrust ball bearing rig (Fafnir Fretting Wear Tester).

Table 2. Test Conditions Employed in the Thrust Ball Bearing Rig.

Variable	Tested values
Oscillation arc length (rad)	0.21
Total load (N)	2450
Max. Hertz pressure in ball-ring contact, p_0 (GPa)	2.41
Oscillation frequency (Hz)	25
Test duration (hours)	22
Test temperature (°C)	25

using simple custom algorithms. This measure was found to be better than mass loss and generally correlated with the maximum wear scar depth, but its consistency depends on the location of the reference plane, and small adjustments in this can have a large influence on the calculated wear volume. Depending on the position of the plane, this measure can pick up the volumes of roughness valleys just outside the contact that are clearly not caused by wear. The maximum wear depth was found to be the most consistent and reliable parameter to describe the observed wear in the HFRR tests and hence was chosen to describe the present results.

Thrust ball bearing rig

Additional tests were performed on a full bearing test rig, commonly referred to as the Fafnir Fretting Wear Tester, which is designed to perform tests according to the ASTM D4170 standard *(19)*, which evaluates "fretting wear protection by lubricating greases." The trends observed on this bearing rig were then compared to those obtained on the HFRR ball-on-disc setup already described. The bearing rig is shown in Fig. 4. The rig oscillates the races of two ball thrust bearings using an offset connecting rod attached to an electric motor. The thrust bearing load is provided through a compressed spring. The eccentricity of the motor attachment defines the oscillation amplitude, the spring force defines the load, and the AC power supply defines the frequency. These are all kept constant in the Fafnir setup to conform to ASTM D4170, and the same standard values were employed in the present tests, except for the frequency, where a 25-Hz power supply was used here, as listed in Table 2. The rig has no means of temperature control and all tests were conducted at room temperature of approximately 25 °C.

Test procedure for thrust ball bearing rig tests

Before testing, the test rig and bearings were cleaned using petroleum ether (PE) followed by isopropyl alcohol (IPA). The bearings were additionally cleaned ultrasonically for 15 minutes in an IPA bath before being allowed to air-dry fully. Individual bearing races as well as each ungreased bearing assembly were then weighed using an analytical balance to the nearest 0.1 mg. The tracks and cages were then filled with 1.00 g ± 0.05 g of test grease.

Each bearing race and cage was assembled into its appropriate location (marked ABCD in Fig. 4) in the chuck, which was then assembled with the load shim, spring guide, spring, spacer, and washer. The connecting rod was then attached to the arm of the oscillating bearing seat. The tests were run for 22 h, with the time being controlled with an on/off automatic time switch.

At the end of the test, the chuck was disassembled and specimens were cleaned using IPA. All four individual bearing races were then reweighed and the total mass loss of the upper race pair and that of the lower race pair were calculated. An average value of the mass loss for a single pair of races was then calculated from these two values. Three tests were completed for each lubricant, and the reported weight loss values are the average across these replicates. Additionally, each wear scar was imaged using a digital microscope.

Test materials and lubricants

In the HFRR tests, both upper (ball) and lower (disc) specimens were made of standard through-hardened AISI 52100 bearing steel with the properties given in Table 3. The modified optical HFRR setup with optical access to the fretting contact had a sapphire disc as the upper specimen and the same bearing steel ball as the lower specimen. The properties of the sapphire disc used in this modified setup are also listed in Table 3.

The specimens for the thrust ball bearing Fafnir rig were LT5/8 thrust ball bearings made of AISI 52100 through hardened bearing steel. As is standard for this setup, small flats were machined onto the side of each bearing race to assist with alignment when mounting onto the rig.

To assess the influence of lubricant properties, a selection of oils and a group of custom-made greases were employed. These are listed in Table 4. These were either pure base oils

Table 3. HFRR test specimen properties (hardness and roughness quoted as measured).

Specimen	Material	Hardness (HV)	Radius (mm)	Ra roughness (nm)
Ball	AISI 52100 steel	850 ± 15	3.00 ± 0.01	40 ± 2
Disc	AISI 52100 steel	755 ± 15	inf	15 ± 2
Sapphire disc	Sapphire	1295 ± 20	inf	10 ± 2

Table 4. Properties of tested oils and greases.

	Designation	Type	Thickener	Base oil	ν at 40 °C, mm^2/s	ν at 100 °C, mm^2/s	NLGI
1	PAO25	Oil	N/A	PAO	26	5	N/A
2	PAO50	Oil	N/A	PAO	48	8	N/A
3	PAO200	Oil	N/A	PAO	211	28	N/A
4	PAO400	Oil	N/A	PAO	413	50	N/A
5	LPAO25	Grease	Lithium	PAO	26	5	2
6	LPAO50	Grease	Lithium	PAO	48	8	2
7	LPAO200	Grease	Lithium	PAO	211	28	3
8	LPAO400	Grease	Lithium	PAO	413	50	2-3
9	UPAO50	Grease	Urea	PAO	48	8	2

(rows 1 to 4) or custom-made greases using the same base oils and either a lithium hydroxystearate or an aliphatic diurea thickener (rows 5 to 9). The film-forming and frictional behavior of these oils and greases is extensively reported in previous publications from the authors' group, namely, in De Laurentis et al. *(22)* and in Kanazawa et al. *(23, 24)*. These lubricants were selected to allow systematic evaluation of the influence of different lubricant properties on false brinelling. The use of pure PAO oils of four differing viscosities listed in rows 1 to 4 allows for the effect of viscosity on fretting damage to be studied (PAO50-PAO400). The use of lithium greases with the same base oils listed in rows 5 to 8 allows for the comparison between the effects of greases and the effects of equivalent base oils on fretting to be studied (LPAO50-400). Finally, the inclusion of both a lithium grease and a urea grease with the same PAO 50 base oil (referred to as LPAO50 and UPAO50 greases, respectively; rows 6 and 9) allows for the influence of the thickener type to be investigated. To allow for a controlled study, none of the lubricants contained any additives, to avoid any additional chemical effects, which are often difficult to track.

Results

Results are presented to first illustrate the way in which the false brinelling damage was seen to initiate and progress. This is then followed by detailed results that illustrate the effect of lubricant properties, stroke length, applied load, and oscillation frequency.

Direct observation of damage onset and progression

The onset and progression of damage was observed in situ using the optical setup on the HFRR employing a sapphire disc oscillating on an AISI 52100 ball. Using this setup, a series of videos looking into the oscillating contact were recorded under different contact conditions. These videos are very helpful in visualizing damage initiation and progression, and the reader is referred to supplementary data for an example. For the purposes of this article, Fig. 5 shows a series of still images taken at different times from the same video and corresponding to an unlubricated fretting test at 1 GPa pressure, 100 Hz oscillation frequency, and 20 μm stroke. The first onset of damage is apparent in the image corresponding to 10 seconds after the start of the test. It is evident that the damage starts at discrete points located close to the edge of the contact area, that is, within the general region that would be referred to as the slip annulus in fretting contacts of ideally smooth surfaces. This initial damage is concentrated on discrete narrow bands along the sliding direction, with lengths approximately equal to the applied stroke length. This suggests that fretting damage first starts due to slipping at selected asperity contacts preferentially located within the annulus of macro-slip. These damage bands are seen to become more numerous and their length progressively longer as the test progresses (see 20 and 30 seconds images). By about 40 seconds the damage has spread to cover most of the contact area including the central part, which is normally considered to be the stick region in an ideally smooth contact. Since this is an unlubricated test, the damage spreads rapidly and a noticeable wear scar is formed in less than 60 seconds under these conditions. Figure 6 shows the equivalent images from a test under the same conditions but now lubricated with the UPAO50 urea grease. The general sequence of events in terms of initiation and progression of damage is similar, with the very first damage again appearing in the local asperity contacts, before spreading to the rest of the contact. However, as may intuitively be expected, the initiation and spread of damage are much slower in this lubricated case than were observed in the unlubricated test of Fig. 5. Now the first damage is seen to occur after about 10 minutes, compared to 10 seconds in the unlubricated condition, and the extent of damage after 60 minutes is less than that after 60 seconds in the unlubricated case.

It should be noted that this optical setup of steel ball on sapphire disc is exclusively used here to observe the general onset and progression of damage in fretting type contacts. Other than the material pair, the contact parameters in this setup are the same or similar as those in the steel ball on steel disc tests shown later: The contact size is similar, with contact diameter being about 80 μm in both cases, the roughness of the sapphire flat is similar to the roughness of the HFRR ball in the steel ball on steel disc tests (10 nm and 15 nm Ra, respectively), and a hardness differential exists between the two bodies in both setups (with the sapphire disc being harder than the steel ball in the optical setup and the ball being harder than the disc in the steel-on-steel setup). However, owing to the differences in tribopair material properties, the absolute amount of damage observed in these optical tests should not be compared to that in the equivalent steel-ball-on-steel-disc tests described in the following. There are also obvious differences in surface chemistry between the sapphire and steel, but this optical setup is not used to compare the fretting resistance of different lubricant formulations or to obtain any quantitative measurements of fretting wear, so this is largely inconsequential.

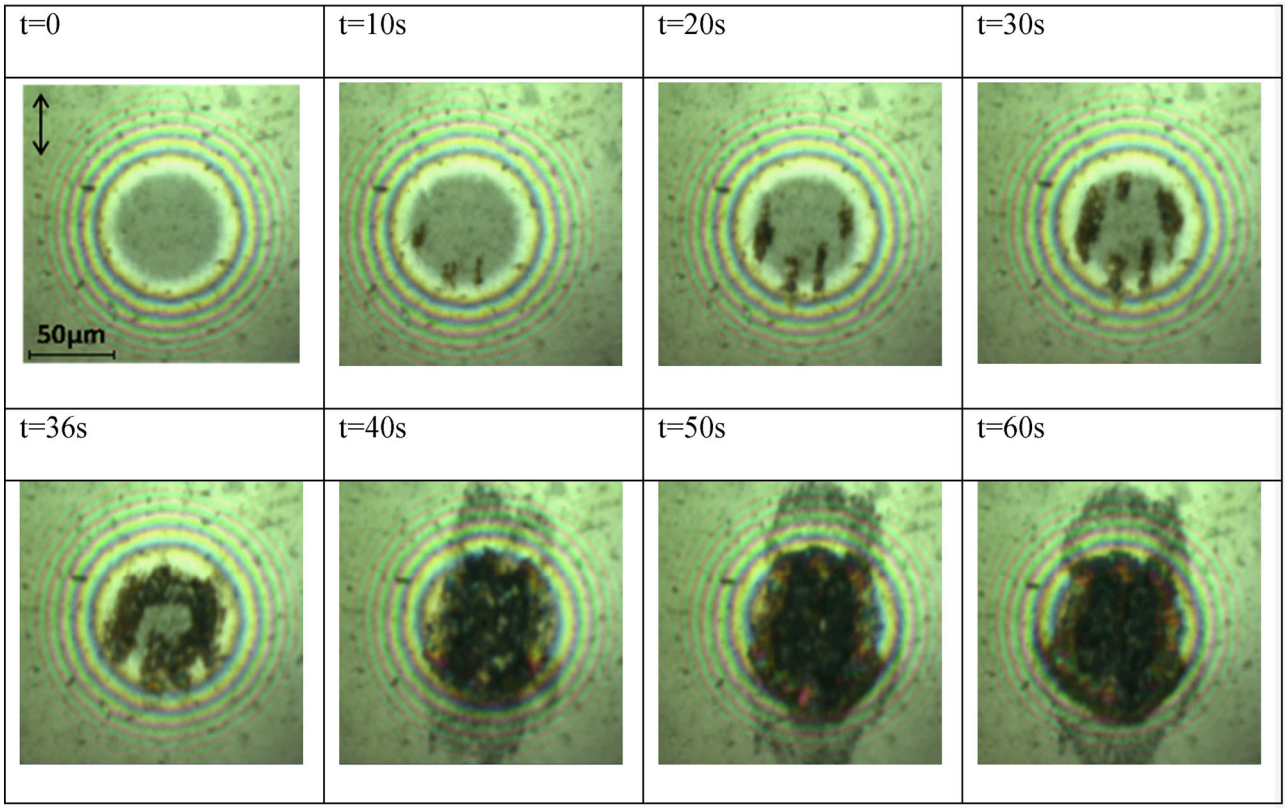

Figure 5. Images illustrating the fretting damage progression observed using the optical HFRR setup (sapphire disc on AISI 52100 steel ball) for an unlubricated test at 100 Hz, 1 GPa, and 20 μm stroke length. Hertzian contact diameter 80 μm. (The scale in the first image applies to all images shown. Direction of imposed motion is up–down in all pictures.)

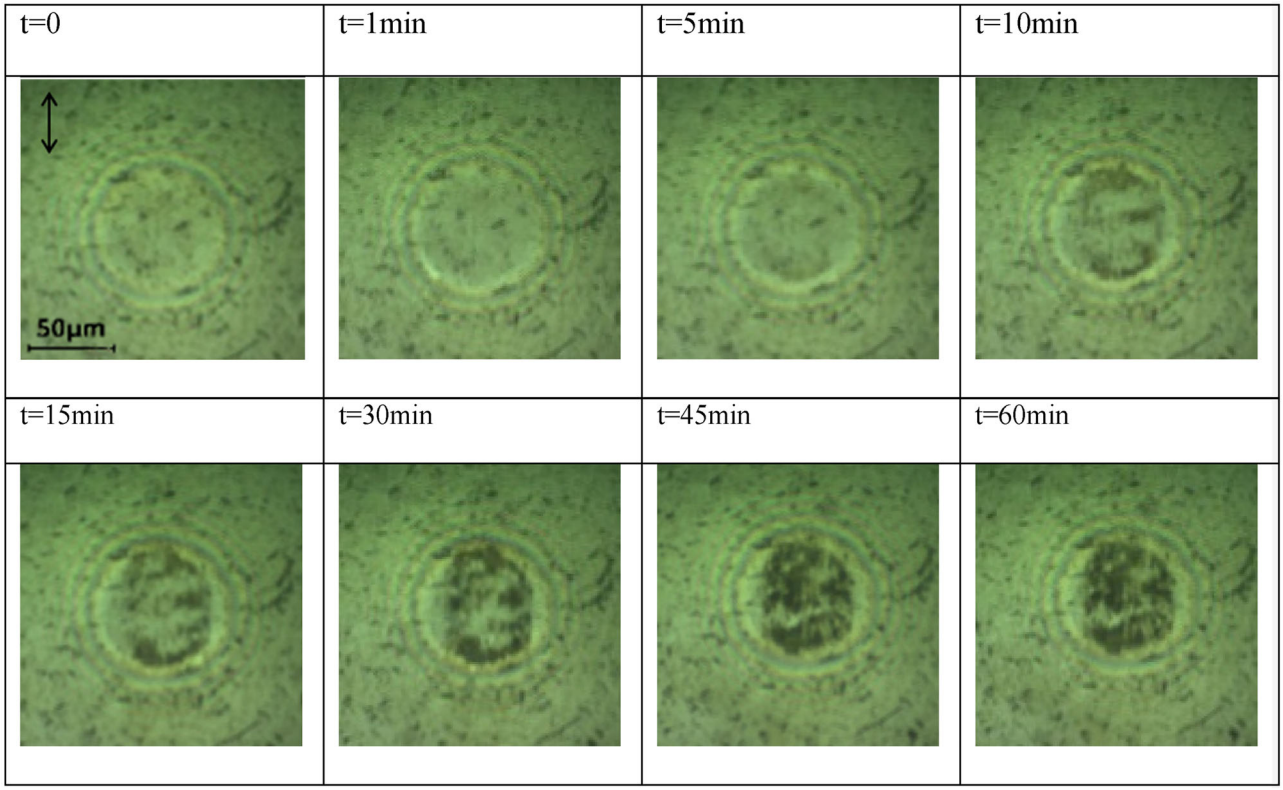

Figure 6. Fretting damage progression observed using the optical HFRR setup (sapphire disc on AISI 52100 steel ball) in a test lubricated with the urea-thickened grease (UPAO50) at 100 Hz, 1 GPa, and 20 μm stroke length. Hertzian contact diameter 80 μm. (The scale in the first image applies to all images shown. Direction of imposed motion is up–down in all pictures.)

Influence of lubricant properties

Influence of base oil viscosity

To investigate the influence of oil viscosity, PAO oils with four different viscosities (25, 50, 200, and 400 cSt at 40 °C), and lithium-thickened greases with the same four PAO base oils were tested in the HFRR rig using AISI 52100 bearing steel balls and discs. Figure 7 shows the wear scar depth, average friction coefficient, and average normalized value of electrical contact resistance obtained in these tests for these PAO oils and lithium greases at 20 μm stoke length, 100 Hz, and 1 GPa. Figure 8 shows the corresponding white light interferometry measurements of the wear scars at the end of typical tests for each of these lubricants. A clear trend is immediately apparent in Fig. 7: The amount of fretting wear increased with the oil viscosity for both oils and greases. Average friction also increased with increasing viscosity in all cases. Figure 9 shows the corresponding evolution of friction over the duration of these same tests for one of the test repeats. This shows that for both greases and base oils, friction throughout the test was generally higher for the two higher oil viscosities (200 cSt and 400 cSt) than for the two lower viscosities (25 cSt and 50 cSt). For the two higher viscosities the absolute value of friction is as high as 0.4 for a considerable amount of time, which is much higher than the friction coefficient that may be expected in boundary lubrication, suggesting that the contact is at times operating under effectively dry conditions. In addition, the friction coefficient at higher viscosities showed a lot of variation throughout the tests particularly for greases, at times rising to 0.4 but falling as low as ~0.15 for short periods of time. In contrast, in the case of the two lower viscosities, the friction coefficient is relatively steady between 0.1 and 0.15 for the duration of the test; these values are what may generally be expected under boundary lubrication. These results

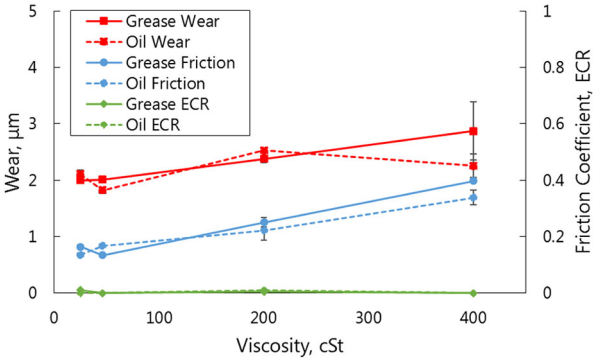

Figure 7. Maximum wear depth, average friction coefficient, and average electrical contact resistance for PAO oils with viscosities of 25, 50, 200, and 400 cSt at 40 °C and lithium-thickened greases with these same base oils. AISI 52100 steel ball on AISI 52100 disc, stroke length 20 μm, Hertz pressure 1 GPa, frequency 100 Hz.

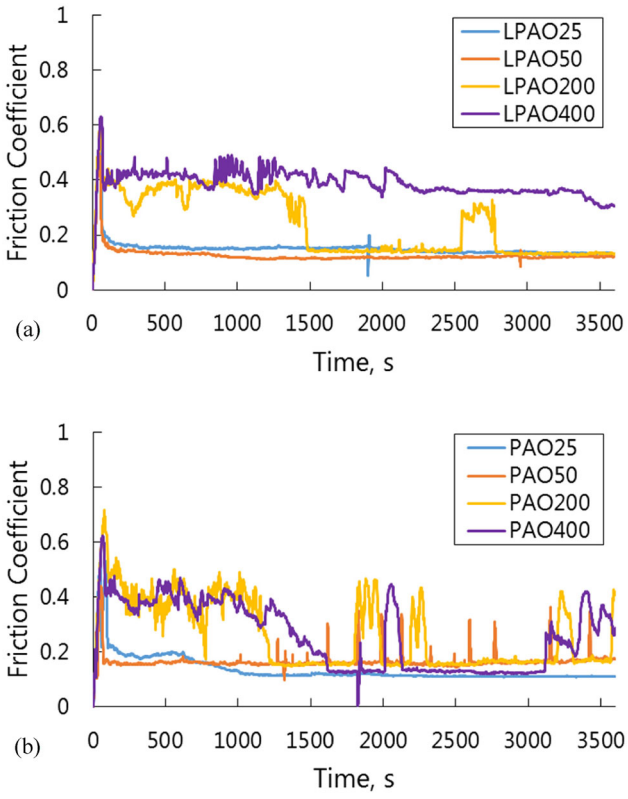

Figure 9. Recorded friction coefficient during typical 1 hour lubricated tests at 1 GPa pressure, 20 μm stroke, and 100 Hz frequency, AISI 52100 steel ball on AISI 52100 disc: (a) lithium-thickened greases with viscosities of 25, 50, 200, and 400 cSt at 40 °C, and (b) corresponding PAO base oils.

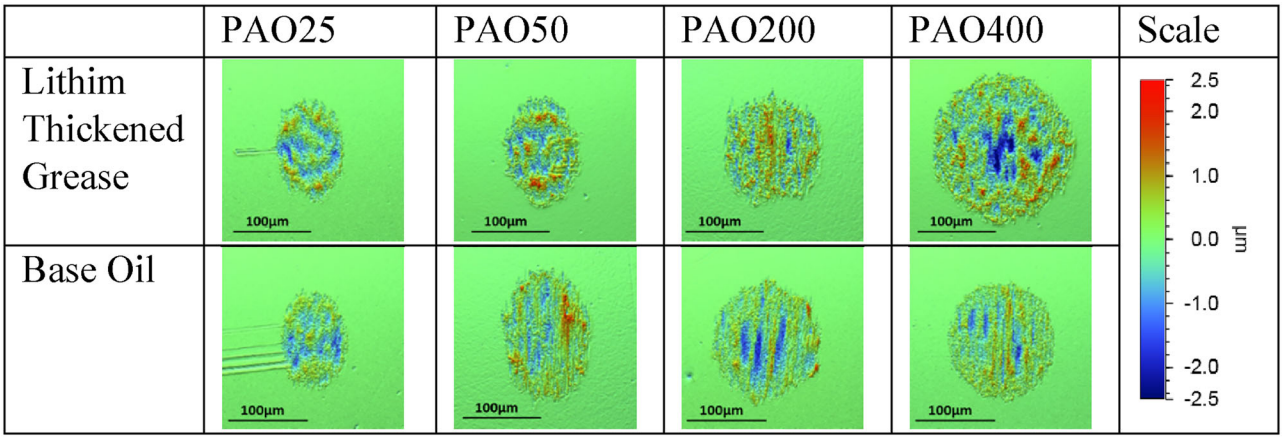

Figure 8. Wear scars measured using white light interferometry at the end of typical 1-hour HFRR test with PAO oils with viscosities of 25, 50, 200, and 400 cSt at 40 °C and lithium-thickened greases with these same base oils. AISI 52100 steel ball on AISI 52100 disc, stroke length 20 μm, Hertz pressure 1 GPa, frequency 100 Hz, Hertzian contact diameter 84 μm.

suggest that the lower viscosity oils are better able to supply the oscillating contact and hence reduce friction and wear, whereas the higher viscosity oils are only able to supply the contact intermittently. However, on average the recorded electrical contact resistance is negligible for all viscosities tested, which indicates that the contact is operating in a boundary regime at best, even in the case of low-viscosity oils. Finally, results also show that the wear and friction were generally slightly lower for the pure PAO oils than for their equivalent lithium greases but the differences are not particularly large.

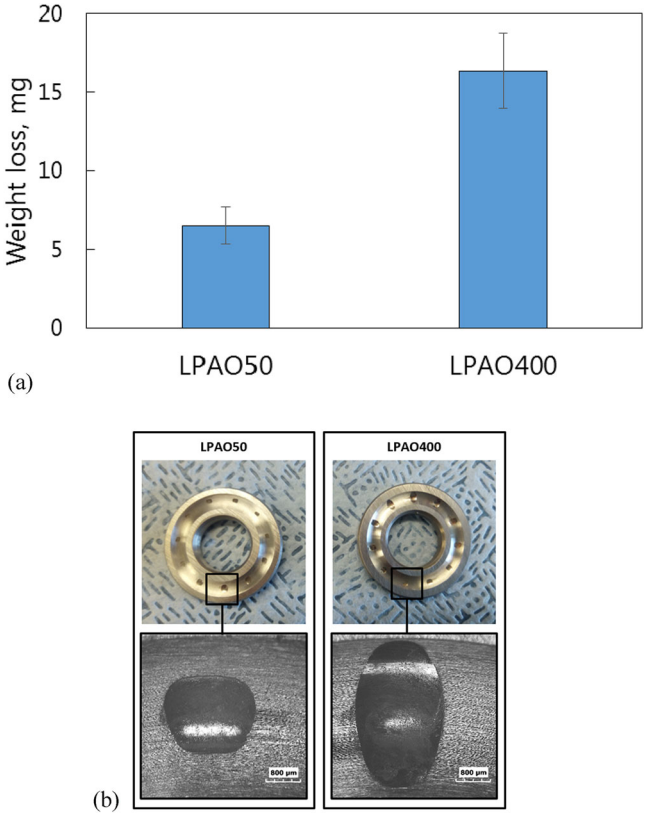

Figure 10. Results of false brinelling tests in thrust ball bearing (Fafnir) rig with LPAO50 and LPA.O400 lithium greases (i.e., base oil viscosities of 50 cSt and 400 cSt at 40 °C, respectively: (a) measured average weight loss of a bearing raceway pair, and (b) typical microscope images of the corresponding wear scars on the bearing raceways.

Influence of oil viscosity in full bearing rig tests

The lithium-thickened LPAO50 and LPAO400 greases were also tested in full bearings using the thrust ball bearing rig described earlier at the conditions listed in Table 2. Figure 10(a) shows the average weight loss of each pair of bearing raceways for both tested greases. The corresponding images of typical wear scars on the bearing raceways are shown in Fig. 10(b). It is evident that the grease with the higher base oil viscosity produced both a higher weight loss and visually larger false brinelling scars on the bearing raceways. These results are in line with the trends observed in the HFRR tests and hence indicate that the observations made in the ball-on-disc HFRR tests are applicable to real bearings, at least in terms of the general trends.

Influence of contact conditions

Influence of stroke length

Figure 11 shows the maximum depth of the final wear track, the average friction coefficient, and the average normalized electrical contact resistance obtained in tests with eight different stroke lengths ranging from 20 μm to 160 μm, with

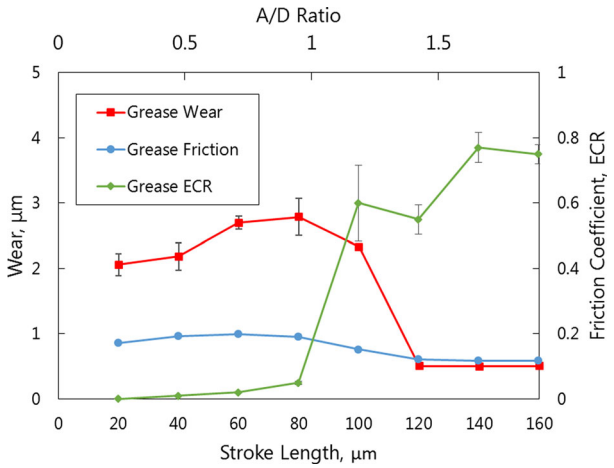

Figure 11. Maximum wear depth, average friction coefficient, and average electrical contact resistance recorded in HFRR tests at eight different stroke lengths from 20 to 160 μm (AISI 52100 steel ball on AISI 52100 disc, 1 GPa, 100 Hz, urea-thickened PAO50 grease, UPAO50).

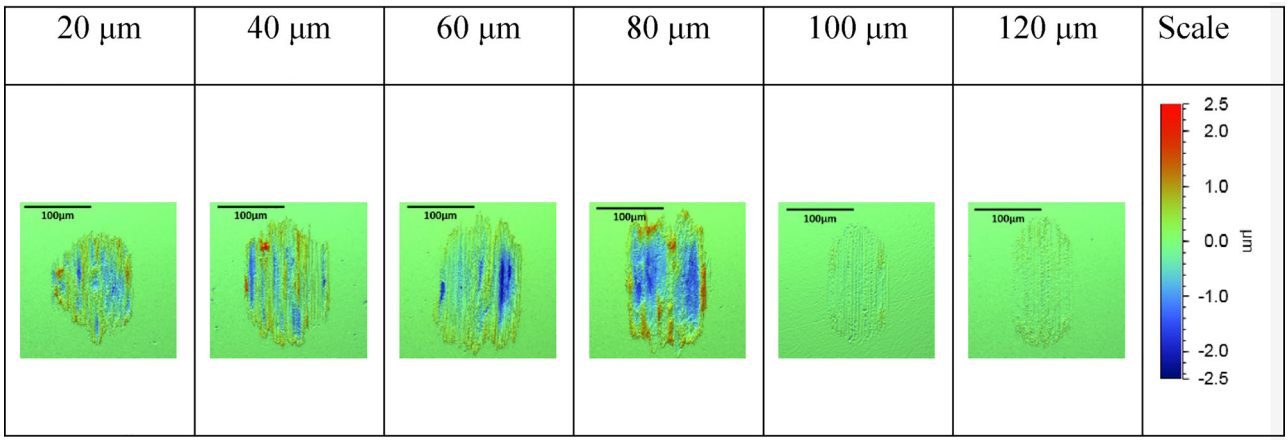

Figure 12. White light interferometry of wear scars at stroke lengths from 20 to 120 μm (AISI 52100 steel ball on AISI 52100 disc, 1 GPa pressure, 100 Hz frequency, urea-thickened PAO50 grease, UPAO50). Corresponding friction and wear results are shown in Fig. 11.

urea-thickened PAO50 grease (UPAO50) at 1 GPa and 100 Hz. The contact size in these tests was 84 μm so that this range of amplitudes covers A/D ratios from 0.25 to just under 2 (A/D ratios are shown on the additional x-axis above the plot) Figure 12 shows the corresponding white light interferometry (WLI) measurements of the typical post-test wear scars for the different stroke lengths. Both friction and wear were relatively similar for all stroke lengths less than 80 μm to 100 μm. However, when stroke length was increased from 100 μm to 120 μm there was a very sharp drop in both wear and friction. At stroke lengths above 120 μm wear and friction were again relatively constant. The average electrical contact resistance signal was zero for all strokes below 80 μm but showed a sharp rise at 100 μm stroke length and continued to rise slightly for yet higher stroke lengths.

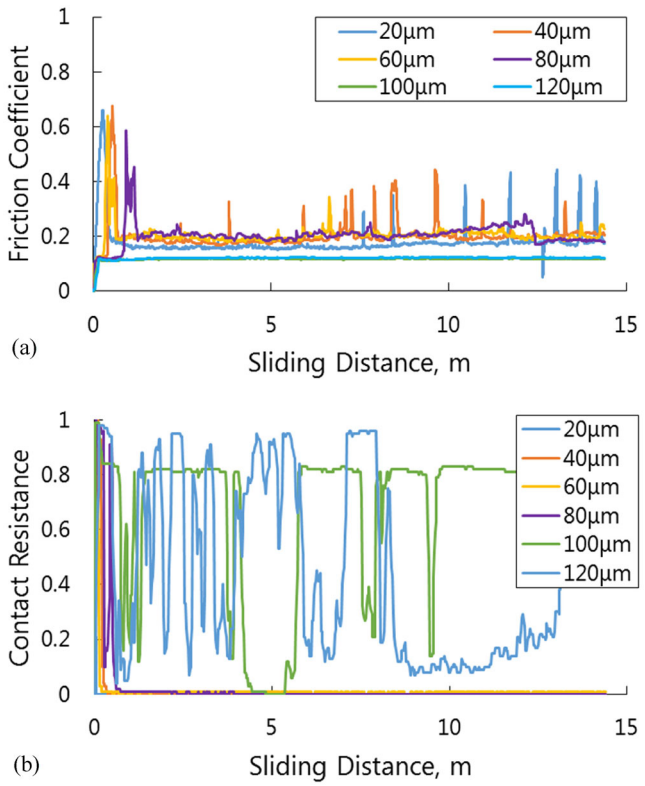

Figure 13. Recorded evolution of (a) friction coefficient and (b) electrical contact resistance during typical tests at six different stroke lengths from 20 to 120 μm (AISI 52100 steel ball on AISI 52100 disc, 1 GPa, 100 Hz, urea-thickened PAO50 grease, UPAO50). Corresponding friction and wear results are shown in Fig. 11.

These results strongly indicate that there was a change in wear mechanism above about 80 μm stroke length, that is, above an A/D ratio of 1. To investigate this further, Fig. 13 shows the evolution of friction and electrical contact resistance with sliding distance during typical tests at stroke lengths ranging from 20 to 120 μm. It is evident that at 100 μm and 120 μm stroke lengths the friction was much lower than at all shorter amplitudes. The electrical contact resistance signal is also seen to be relatively high at 100 μm and 120 μm for much of the test, with only momentary dips to lower values (Fig. 13b), suggesting that under these conditions there is a lubricant film present within the contact most of the time. In contrast, the electrical contact resistance was zero at all times for stroke lengths of 80 μm and less, indicating that metal-to-metal contact was present.

The apparent trends identified here are further supported by the corresponding observations on the optical HFRR setup. Figure 14 shows a series of images at different times for the tests at 20 and 100 μm stroke lengths. Very little wear is seen by 60 minutes in the test at 100 μm stroke length, whereas damage is initiated within 10 minutes in the test at 20 μm. In addition, the images of the test at 100 μm stroke length show the contact as a very bright area, distinctly different from the equivalent images at 20 μm, which may indicate the increased presence of lubricant in the contact, in line with the ECR results of Fig. 13.

Figure 15 shows force–displacement charts, also known as fretting loops, recorded at 60 seconds test time for the same tests at 20 μm and 100 μm stroke length lubricated with urea-thickened PAO50 grease (UPAO50) at 1 GPa and 100 Hz. At 20 μm (A/D $\approx$ 0.25), the force–displacement "loop" is mostly closed. This indicates that the contact is in the partial slip regime with the imposed displacement mostly accommodated by the elastic deformation within the contact

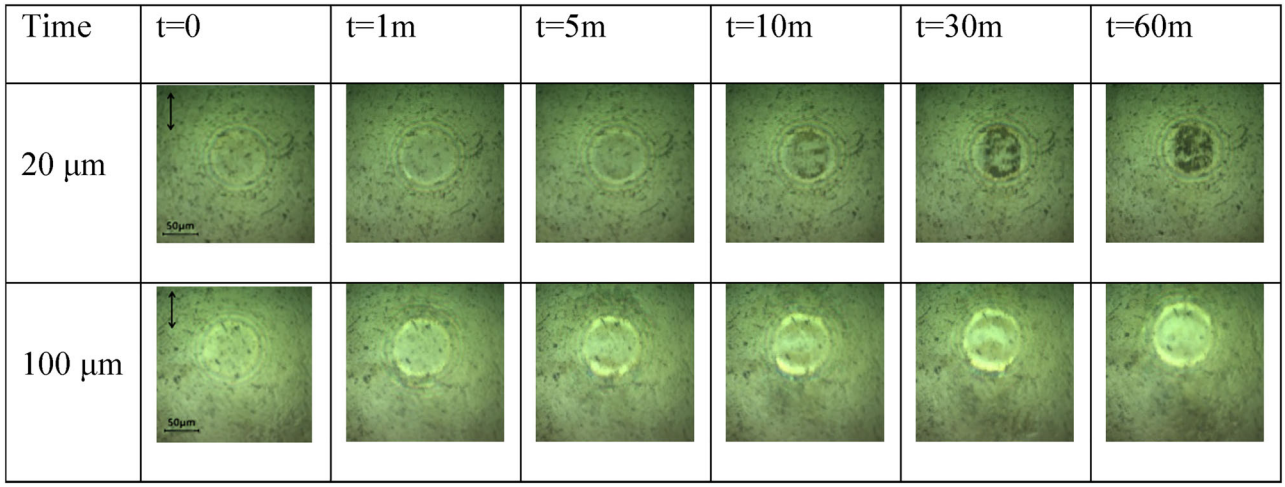

Figure 14. Fretting damage progression observed using the optical HFRR setup (sapphire disc on AISI 52100 steel ball) in tests at 20 μm and 100 μm lubricated with urea-thickened grease UPAO50, 100 Hz frequency, and 1 GPa pressure. (Direction of imposed motion is up–down in all pictures.)

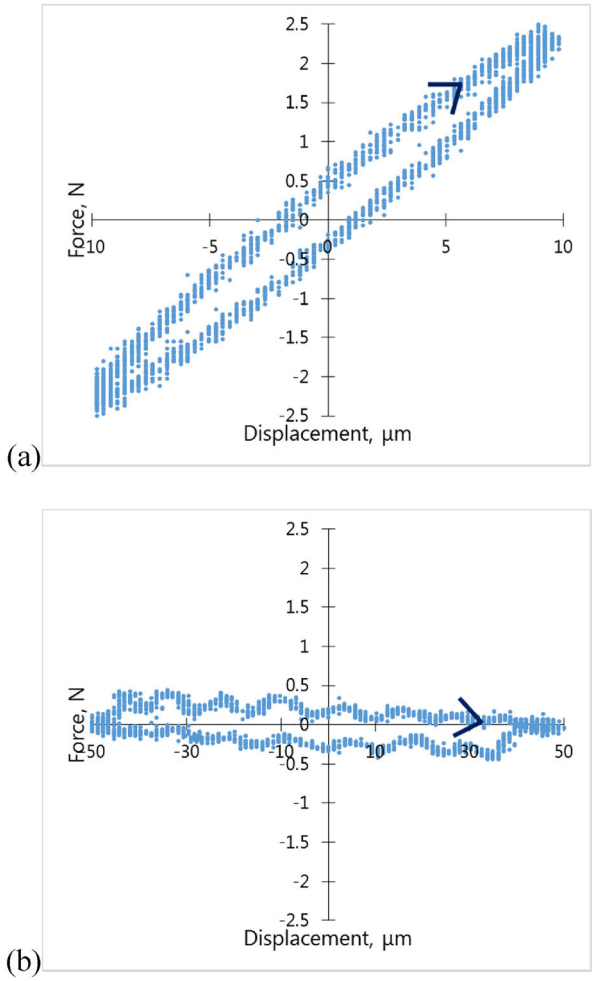

Figure 15. Plots of instantaneous tangential force against displacement (relative to mid-stroke point) for a single oscillation ("fretting loops") obtained at 60 seconds after start of tests: (a) stroke length 20 μm (A/D $\approx$ 0.25) and (b) stroke length 100 μm (A/D $\approx$ 1.20) (AISI 52100 steel ball on AISI 52100 steel disc, pressure 1 GPa, frequency 100 Hz, urea-thickened PAO50 grease, UPAO50). In both cases the stroke reversal occurs at the extremes of the relative displacement shown on the *x*-axis.

with little gross slip occurring, as may be expected at this low A/D ratio. The tangential force therefore increases linearly with imposed displacement, and upon reversal it starts reducing again, until it changes sign once the mid-stroke point is reached; that is, the elastic deformation starts to increase in the other direction. In contrast, at 100 μm stroke length (A/D $\approx$ 1.20) the recorded loop indicates that gross slip is taking place between the contacting surfaces. The tangential force (friction) now remains constant once slip starts, and it changes direction at the point of stroke reversal. These observations further support the assertion that prevalent tribological conditions are very different in the two cases and that a different wear mechanism existed at stroke lengths larger and smaller than the contact diameter.

Influence of contact pressure

Figure 16 shows final wear scar depth, average friction coefficient, and average electrical contact resistance in HFRR tests at contact pressures of 0.65, 0.82, 1.04, and 1.30 GPa. All tests were conducted at 20 μm stroke, 100 Hz, and with

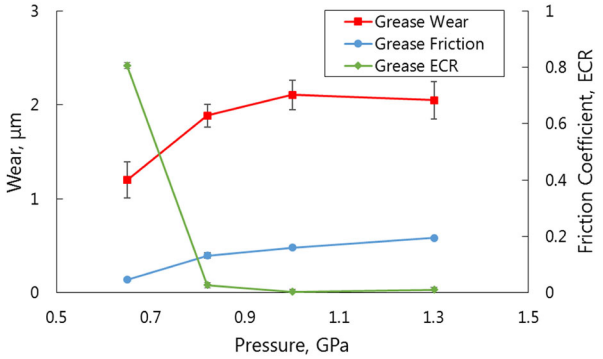

Figure 16. Maximum wear depth, average friction coefficient, and average electrical contact resistance (ECR) recorded in HFRR tests at different contact pressures, 0.65, 0.82, 1.04, and 1.30 GPa (urea-thickened UPAO50 grease, 20 μm stroke, 100 Hz, AISI 52100 steel ball on AISI 52100 steel disc).

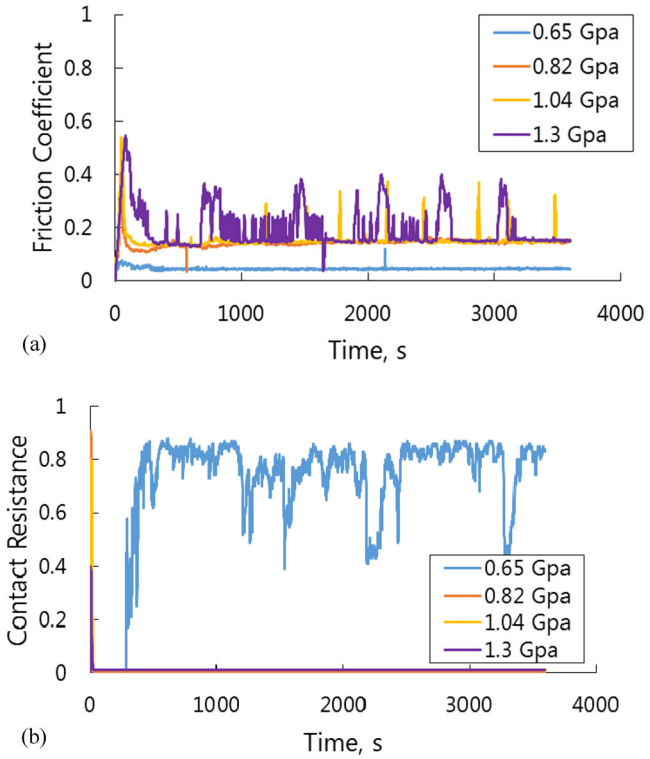

Figure 17. Recorded evolution of (a) friction coefficient and (b) electrical contact resistance during typical lubricated tests at different Hertz contact pressures, for urea-thickened grease with PAO50 base oil, 20 μm stroke length, and 100 Hz frequency.

the urea-thickened grease, UPAO50. At the lowest pressure of 0.65 GPa, friction and wear were much lower than at all other pressures. As pressure was increased from 0.65 GPa to 0.82 GPa, there is a clear increase in both friction and wear, but as the pressure increases further to 1.04 GPa and 1.30 GPa, friction and wear remain relatively steady. The electrical contact resistance (ECR) signal shown in Fig. 17(b) remained above zero throughout the test at 0.65 GPa, indicating that practically a full separation of the surfaces is achieved by a lubricant film present throughout the entire duration of the test. In contrast, at all higher pressures tested here, the ECR signal is negligible, indicating metal-to-metal contact throughout the test. This is further supported by the friction traces shown in Fig. 17(a), where it is evident

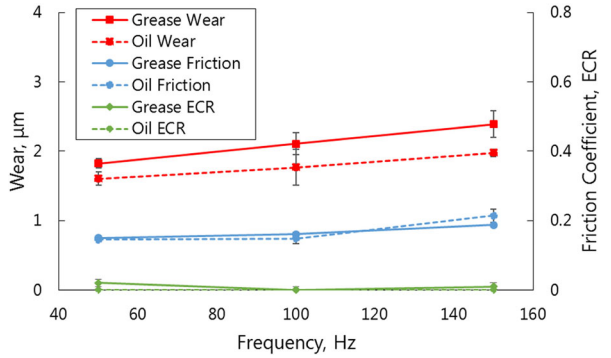

Figure 18. Friction coefficient, wear depth, and electrical contact resistance for frequencies of 50 Hz, 100 Hz, and 150 Hz; stroke length 20 μm, pressure 1 GPa, and PAO50 oil and urea-thickened UPAO50 grease as lubricant.

that the friction coefficient was steady at around 0.05 for pressure of 0.65 GPa, whereas it was generally higher than 0.15 and shows numerous spikes as high as 0.4 in tests at all higher pressures. The existence of lubricant film throughout the test duration at 0.65 GPa suggests that the lubricant was never completely pushed out of the contact, thus leading to reduced friction and wear even at these very small A/D ratios. At higher pressures the oscillations in the ECR and friction suggests that lubricant is at times pushed out of the contact but is able to re-flow back intermittently.

It should be noted that when contact pressure is varied with this fixed geometry, the Hertz contact diameters are also changed, ranging from 55 μm (A/D $\approx$ 0.36) at 0.65 GPa to 110 μm at 1.3GPa (A/D $\approx$ 0.18). However, this is very unlikely to be the reason for the observed trends given that the biggest difference occurs between 0.65 GPa and 0.82 GPa where A/D reduces only slightly from 0.36 to 0.28, and that for all pressures tested here the A/D ratio is less than 0.36 and wear and friction were earlier shown to be very similar for all A/D ratios less than 1.

A series of images showing fretting damage progression at these same pressures obtained in the optical HFRR setup is included in the Supplementary Data. These show that the damage initiates earlier and is more extensive at the end of the test at the higher contact pressures.

Influence of frequency

Figure 18 shows the maximum wear depth, average friction coefficient, and normalized electrical contact resistance (ECR) recorded in HFRR tests at oscillating frequencies of 50 Hz, 100 Hz, and 150 Hz using PAO50 oil and the corresponding urea-thickened grease. All tests are at a stroke length of 20 μm and pressure of 1 GPa. To ensure valid comparison between tests at different frequencies, all tests were run for the same number of cycles (360,000) by adjusting the test duration. The results show that for both oil and grease, wear scar depth and friction increase with increasing frequency. The friction coefficient was higher than 0.15 in all cases and there was negligible contact resistance present at all frequencies, both of which indicate that no separating lubricant film was formed in any of the tests and metal-to-metal contact prevailed.

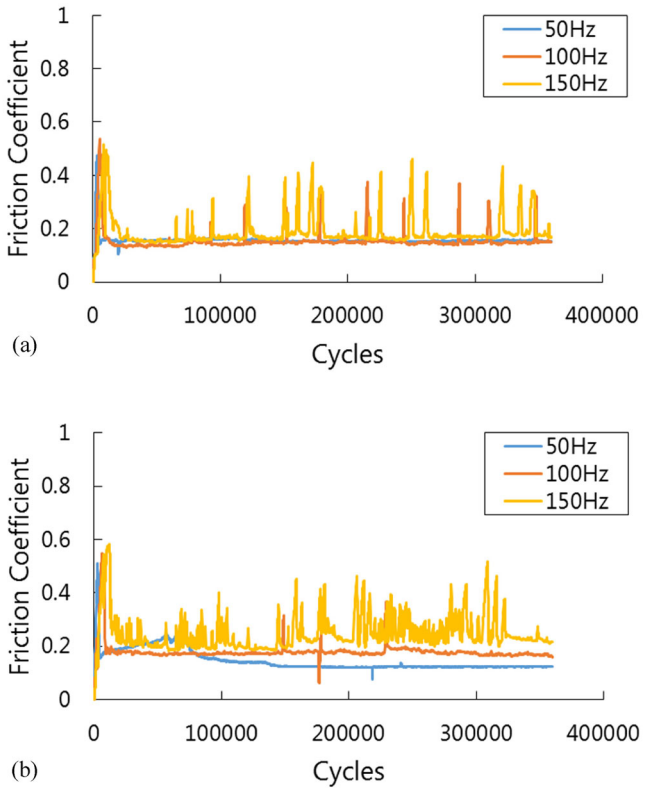

Figure 19. Recorded evolution of friction coefficient during a typical 360,000-cycle lubricated test at 1 GPa pressure and 20 μm stroke: (a) urea-thickened UPAO50 grease and (b) PAO50 base oil.

Figure 19 shows the evolution of the friction coefficient at each frequency throughout the test duration. The most striking feature of these plots is that at the highest frequency of 150 Hz, friction was very unsteady with numerous spikes occurring where friction momentarily jumps to 0.4–0.5 from its base value of about 0.15. This suggests that at 150 Hz there are periods of time when the lubricant supply to the contact is very limited and the contact is operating under almost dry conditions. At 50 Hz and 100 Hz the friction coefficient was relatively steady around the same baseline value of 0.15, indicative of boundary lubrication.

Images of the damage progression at 50 Hz and 150 Hz for PAO50 oil obtained on the optical HFRR setup are included in the Supplementary Data and confirm that damage starts earlier and progresses more quickly at the higher frequency. In addition, the influence of frequency was also tested at a higher oil viscosity of 400 cSt and the same trend was observed. These results are also included in the Supplementary Data.

Discussion

Results presented here show that for oscillating amplitudes less than the contact dimension in the sliding direction (A/D ratios less than 1) lower viscosity oils, lower pressures, and lower frequencies reduce the amount of false brinelling damage. In addition, oils produce less damage than their equivalent greases. These results point to one consistent trend: that the ability of the oil to penetrate the oscillating contact is the key variable that governs the amount of

damage in false brinelling and generally in lubricated fretting. Lower viscosity improves the oil flow and hence increases the amount of the oil that may enter the contact. Lower frequencies mean that there is more time between the stroke reversals for the oil to resupply the swept area, and the lower pressures help the retention of the oil within the contact. However, the electrical contact resistance and friction evolution show that even when the oil does manage to penetrate the contact, no appreciable hydrodynamic film is formed under these low oscillation amplitudes; instead, this limited supply of oil may mean that boundary lubrication may take place rather than contact effectively operating under dry conditions, which appears to be the case with higher viscosities, frequencies, and pressures. This means that it is the flow properties of the oil rather than its film-forming ability that are key to reducing the fretting damage for A/D $<$ 1. Indeed, owing to their superior flow properties the base oils here were shown to result in less damage than their corresponding lithium- and urea-thickened greases despite the fact that these grease were previously shown to form much thicker films then the oils under low speeds and standard unidirectional rolling sliding conditions *(25–27)*.

The amplitude of oscillation was shown to be a crucial factor in false brinelling, in line with other fretting wear studies *(2, 25, 26)*. A drastic reduction in damage was seen when the A/D ratio exceeded 1. The reason for this is likely to be due to the fact that at A/D $<$ 1 there exists a central region of the contact that is never exposed to the surroundings and hence may not be reached by the oil at all. Even if it is assumed that the oil is successfully entrained through conventional mechanisms in the inlet of an oscillating contact, for A/D $<$ 1 the direction of motion is reversed before this oil is able to reach the central region of the contact so that this region probably operates under nearly dry conditions. This is in line with observations made by Zhou et al. *(27)*, who observed more severe damage in the centre of a fretting contact. Clear evidence for lack of lubricant penetration for A/D $<$ 1 is here provided by the electrical contact resistance and friction measurements, which show that no separating oil film is present in the contact and that friction is at times higher than what may be expected under boundary lubrication, intermittently reaching as high as 0.4, which is indicative of a nearly dry steel-on-steel contact. Increasing the oscillating amplitude to A/D $>$ 1 is likely to have two beneficial effects: First, it promotes lubricant entrainment into the contact so that some hydrodynamic film may actually form in this case, and second, it makes it easier for any iron oxide debris formed to be ejected from the contact, although this latter effect was not studied here. The potential existence of a hydrodynamic film for A/D $>$ 1 was here evidenced by the electrical contact resistance and friction measurements. This in turn means that for A/D $>$ 1, the properties of the lubricant that promote hydrodynamic film formation, such as higher viscosity, may actually decrease false brinelling damage, in contrast to what happens for A/D $<$ 1. Indeed, Maruyama et al. *(28)* have shown that for A/D $>$ 1.6, higher oil viscosity reduces friction.

Therefore, the potential mitigating measures against false brinelling depend on the amplitude of oscillation, with lower viscosity, more mobile oils, and lower frequencies (and hence lower speeds) reducing damage at A/D $<$ 1, whereas higher viscosity and higher speeds may better mitigate against damage when A/D is greater than 1.

In-situ observations of the onset and progression of false brinelling using the optical HFRR setup indicate that damage initially starts at discrete asperity contacts in the form of narrow bands of wear approximately equal in length to the applied oscillating amplitude. With further cycles, the damage spreads to cover the rest of the contact area. This indicates that the conditions in asperity contacts and hence surface roughness properties play an important role in damage onset and that therefore, optimizing the surface roughness structure may also provide an effective mitigating measure against false brinelling.

Conclusions

This study investigated the effects of lubricant properties and contact conditions on false brinelling damage using a ball-on-disc high-frequency reciprocating rig (HFRR). AISI 52100 bearing steel specimens and a selection of PAO oils with differing viscosities, and custom-made lithium and urea greases with the same base oils were employed. An additional adaptation to the HFRR setup employing a sapphire disc on a steel ball enabled optical access to the contact and hence direct observation of the onset and progression of false brinelling damage. Finally, additional tests were conducted on a thrust ball bearing rig with the same lubricants. The main findings can be summarized as follows:

- False brinelling damage initiates in discrete asperity contacts in the form of narrow wear bands approximately equal in length to the applied oscillation amplitude. The damage then spreads relatively quickly to the rest of the contact.
- Results confirm that the oscillation amplitude has a major effect on the amount of damage, with the amplitudes shorter than the Hertz contact width in the sliding direction (A/D $<$ 1) being most damaging, while a drastic reduction in damage was observed for all amplitudes larger than the contact width (A/D $>$ 1). Electrical contact resistance and friction measurements indicate that for A/D $<$ 1 the contact operates in boundary lubrication at best, with a friction coefficient of around 0.1, but intermittently friction reaches as high as 0.4, indicating that the contact is almost dry for short periods of time. In sharp contrast, for A/D $>$ 1 some separating hydrodynamic film appears to be present leading to lower friction and wear.
- In the case of short amplitudes where A/D $<$ 1, the following trends were observed:
  - Lower viscosity oils and greases with lower viscosity base oils significantly reduce the amount of false brinelling damage.
  - Base oils generally produced somewhat less damage than their corresponding greases. This is despite the

fact that these greases were previously shown to build thicker films than the base oils under low speeds.
  - The lowest pressure tested here, 0.65 GPa, resulted in much less damage than all higher pressures.
  - Lower oscillation frequencies resulted in less damage.
  - Electrical contact resistance and friction measurements during these tests show that lubrication conditions are improved by lower viscosities, pressures, and frequencies. However, the contact is still operating in boundary lubrication with no appreciable separating film present between the surfaces. In contrast, higher viscosities, pressures, and frequencies appear to cause the contact to intermittently operate under almost dry conditions, with the friction coefficient being as high as 0.5 for short periods.
- Together, these observations indicate that when oscillation amplitude is shorter than contact width (A/D < 1), the ability of the lubricant to penetrate the contact is a key parameter controlling the amount of damage. Lubricant properties and contact conditions that promote flow of lubricant into the oscillating contact, such as lower viscosities, pressures, and frequencies, reduce the amount of damage. In contrast, when oscillating amplitude is longer than the contact width (A/D > 1), properties of lubricant and contact conditions that promote hydrodynamic film buildup, such as higher viscosities and speeds, may be beneficial in reducing damage.
- The trends and insights presented here may help in devising measures for reduction of false brinelling damage in practical situations.

ORCID

Amir Kadiric http://orcid.org/0000-0002-1342-3470

References

(1) Pittroff, H. (1965), "Fretting Corrosion Caused by Vibration With Rolling Bearings Stationary," *J. Fluids Eng.*, **87**(3), pp 713–723. 10.1115/1.3650657
(2) Grebe, M. (2012), "False Brinelling—Standstill Marks at Roller Bearings," Slovak University of Technology in Bratislava.
(3) Almen, J. O. (1937), "Lubricants and False Brinelling of Ball and Roller Bearings," *Mech. Eng.*, **59**(6), pp 415–422.
(4) Lee-Prudhoe, I., Sayles, R. S., and Kadiric, A. (1999), "Investigations Into Asperity Persistence in Heavily Loaded Contacts," *J. Tribol.*, **121**(3), pp 441–448. 10.1115/1.2834087
(5) Errichello, R. (2004), "Another Perspective: False Brinelling and Fretting Corrosion," *Tribology and Lubrication Technology*, **60**(4), pp 34–36.
(6) Schwack, F., Bader, N., Leckner, J., Demaille, C., and Poll, G. (2020), "A Study of Grease Lubricants Under Wind Turbine Pitch Bearing Conditions," *Wear*, **454**(455), pp 1–15. 10.1016/j.wear.2020.203335
(7) Niizato, T. (2017), "The Technology Trend of Power Train and Expectation on Tribology," in *TTRF-TAIHO International Symposium on Automotive Tribology*.
(8) Taylor, R. I. (2021), "Energy Efficiency, Emissions, Tribological Challenges and Fluid Requirements of Electrified Passenger Car Vehicles," *Lubr. 2021*, **9**(7), p 66.
(9) Campbell, W. E. (1952), "The Current Status of Fretting Corrosion," in *Symposium on Fretting Corrosion*, pp 3–23.
(10) Shima, M., Suetake, H., Mccoll, I. R., Waterhouse, R. B. B., and Takeuchi, M. (1995), "On the behaviour of an oil lubricated fretting contact," *Wear*, **210**(1), pp 304–310. 10.1016/S0043-1648(97)00078-1
(11) Zhou, Z. R. R., and Vincent, L. (1995), "Mixed Fretting Regime," *Wear*, **181**(183), pp 531–536. 10.1016/0043-1648(95)90168-X
(12) Maruyama, T., and Saitoh, T. (2010), "Oil Film Behavior Under Minute Vibrating Conditions in EHL Point Contacts," *Tribol. Int.*, **43**(8), pp 1279–1286. 10.1016/j.triboint.2009.11.004
(13) Söderberg, S., Bryggman, U., and McCullough, T. (1986), "Frequency Effects in Fretting Wear," *Wear*, **110**(1), pp 19–34. 10.1016/0043-1648(86)90149-3
(14) Kirk, A. M., Shipway, P. H., Sun, W., and Bennett, C. J. (2019), "The Effect of Frequency on Both the Debris and the Development of the Tribologically Transformed Structure During Fretting Wear of a High Strength Steel," *Wear*, **426**(427), pp 694–703. 10.1016/j.wear.2018.12.035
(15) Waterhouse, R. B. B. (1955), "Fretting Corrosion," *Proc. Inst. Mech. Eng.*, **169**(1), pp 1157–1172. 10.1243/PIME_PROC_1955_169_112_02
(16) Haviez, L., Fouvry, S., Toscano, R., and Yantio, G. (2015), "An Energy-Based Approach to Understand the Effect of Fretting Displacement Amplitude on Grease-Lubricated Interface," *Wear*, **338–339**(1), pp 422–429. 10.1016/j.wear.2015.07.015
(17) Warmuth, A. R., Sun, W., and Shipway, P. H. (2016), "The Roles of Contact Conformity, Temperature and Displacement Amplitude on the Lubricated Fretting Wear of a Steel-on-Steel Contact," *R. Soc. Open Sci.*, **3**(10), pp 1–28. 10.1098/rsos.150637
(18) Dobromirsk, J. M. "Variables of Fretting Process Are There 50 of Them?"
(19) ASTM (2011), "ASTM D4170: Standard Test Method for Fretting Wear Protection by Lubricating Greases," *ASTM Stand.* **5**, pp 6–11.
(20) Viesca, H. A., Battez, J. L., González, A. H., Reddyhoff, R., Pérez, T., and Spikes, A. T. (2010), "Assessing Boundary Film Formation of Lubricant Additivised With 1-Hexyl-3-Methylimidazolium Tetrafluoroborate Using ECR as Qualitative Indicator," *Wear*, **269**(1–2), pp 112–117. 10.1016/j.wear.2010.03.014
(21) Baker, R. F. (2005). *Durability of steel spline couplings*, PhD Thesis, Imperial College London.
(22) De Laurentis, N., Kadiric, A., Lugt, P. M., and Cann, P. (2016), "The Influence of Bearing Grease Composition on Friction in Rolling/Sliding Concentrated Contacts," *Tribol. Int.*, **94**(1), pp 624–632. 10.1016/j.triboint.2015.10.012
(23) Kanazawa, Y., Sayles, R. S., and Kadiric, A. (2017), "Film Formation and Friction in Grease Lubricated Rolling-Sliding Non-Conformal Contacts," *Tribol. Int.*, **109**(1), pp 505–518. 10.1016/j.triboint.2017.01.026
(24) Kanazawa, Y., De Laurentis, N., and Kadiric, A. (2019), "Studies of Friction in Grease-Lubricated Rolling Bearings Using Ball-on-Disc and Full Bearing Tests Studies of Friction in Grease-Lubricated Rolling Bearings Using Ball-on-Disc and Full Bearing Tests," *Tribol. Trans.* 10.1080/10402004.2019.1662147
(25) Zhou, Z. R. R., Nakazawa, K., Zhu, M. H. H., Maruyama, N., Kapsa, P., and Vincent, L. (2006), "Progress in Fretting Maps," *Tribol. Int.*
(26) Grebe, M., Molter, J., Schwack, F., and Poll, G. (2018), "Damage Mechanisms in Pivoting Rolling Bearings and Their Differentiation and Simulation," *Bear. J.*, **3**(1), pp 71–86.
(27) Zhu, M. H. H., and Zhou, Z. R. R. (2011), "On the Mechanisms of Various Fretting Wear Modes," *Tribol. Int.*, **44**(11), pp 1378–1388. 10.1016/j.triboint.2011.02.010
(28) Maruyama, T., Saitoh, T., and Yokouchi, A. (2017), "Differences in Mechanisms for Fretting Wear Reduction between Oil and Grease Lubrication," *Tribol. Trans.*, **60**(3), pp 497–505. 10.1080/10402004.2016.1180469